Maximum Dynamic Range Operation of a Microwave External Modulation Fiber-Optic Link

Edward Ackerman, *Member, IEEE,* Stephen Wanuga, *Fellow, IEEE,* Dumrong Kasemset, *Member, IEEE,* Afshin S. Daryoush, *Senior Member, IEEE,* Naranjan R. Samant, *Student Member, IEEE*

Abstract— **We fully analyze the analog performance of an external modulation fiber-optic link. We express relevant figures of merit—including gain, noise figure, third-order intermodulation distortion, AM compression, and dynamic range—in terms of the microwave scattering matrices of the modulator and detector circuits, and we predict the modulator bias condition promoting optimum link performance. Our predictions match the measured gain, noise figure, and dynamic range of an experimental 870–930 MHz external modulation fiber-optic link. Maximum spurious-free dynamic range—77 dB · $MHz^{2/3}$ (117 db · $Hz^{2/3}$)—occurs when the modulator is biased at its halfwave voltage, where the optical throughput is nearly pinched off.**

I. Introduction

In medium- and long-haul telecommunications systems and local area networks, fiber-optic links offer many advantages compared to coaxial cables and other metallic waveguides; these include low attenuation at high data rates, low susceptibility to electromagnetic interference, small size, light weight, and compatibility with optical processing schemes. To realize these benefits in a microwave or millimeter-wave phased array, there is now a considerable development effort focused on improving the microwave performance of the fiber-optic links that interconnect high-fidelity communications subsystems in the array [1].

The use of $LiNbO_3$ integrated optical devices to modulate the light in optical waveguides has produced microwave fiber-optic links with high gain and very broad dynamic range. Betts *et al.* [2] reported 11 dB of gain and a spurious-free dynamic range of 104 dB in a 10 Hz bandwidth (i.e., 71 dB · $MHz^{2/3}$ or 111 dB · $Hz^{2/3}$) for a 60 MHz fiber-optic link employing a lumped-element interferometric modulator. A modulator with a traveling-wave electrode structure imparted comparable dynamic range and 35 dB insertion loss to a 20 GHz fiber-optic link [3]. We have demonstrated 0 dB of microwave gain for a 900 MHz external modulation link in which the modulator was biased as its "linear" quarterwave bias point. We had predicted this performance using a signal flow diagram modeling technique which we developed [4]. However, we had not emphasized how the model allows us to also predict the effect of the modulator dc bias voltage upon the link's spurious-free dynamic range.

Kolner and Bloom [5] modeled the effects of biasing the modulator away from its quarterwave voltage, and at a given input signal power they plotted the external modulation link's signal-to-noise ratio, S/N, and minimum detectable signal voltage, $V_{\min}$, as a function of the dc modulator bias. They also predicted the limits to S/N imposed by the modulator's nonlinearity (these limits define CDR, the compression dynamic range), but not the extent to which this nonlinearity creates harmonics resulting in intermodulation distortion that also limits S/N (and defines SFDR, the spurious-free dynamic range). Bulmer and Burns [6] defined and thoroughly investigated intermodulation distortion and spurious-free dynamic range for an external modulation link, but did not predict superior performance resulting from a nonquarterwave modulator bias voltage. Kolner and Dolfi [7] later added the intermodulation distortion effect to the model in [5] and predicted optimum modulator performance, including spurious-free dynamic range, at a bias level comparable to the halfwave switching voltage. Their quantitative predictions were only accurate, however, at frequencies for which the impedance discontinuity at the input to their electro-optic modulator was 50 Ω → 22 Ω.

We model the effect of the modulator bias voltage on link performance using the microwave scattering parameters of our modulator and detector circuits, which we can determine at any frequency from straightforward manipulations of network analyzer measurements [4]. In this paper, we present a comprehensive microwave analysis of external modulation link performance as a function of frequency, including the effect of operating the modulator away from its quarterwave bias point where most results have been reported. We predict the optimum bias voltage at which to operate an $LiNbO_3$ lumped-element Mach–Zehnder interferometric device modulating the optical carrier supplied by a Nd:YAG ($\lambda = 1.3\ \mu m$) laser. Predictions we have made using this model agree with the measured analog performance of an experimental 870–930 MHz external modulation link.

Manuscript received June 6, 1991; revise December 14, 1992.

E. Ackerman, S. Wanuga, and D. Kasemset are with GE Aerospace, Electronics Laboratory, General Electric Company, Syracuse, NY 13221-5840.

A. Daryoush is with the department of Electrical and Computer Engineering, Drexel University, Philadelphia, PA 19104.

N. R. Samanant is with Jaret Communications, Philadelphia, PA 19106.

IEEE Log Number 9210216.

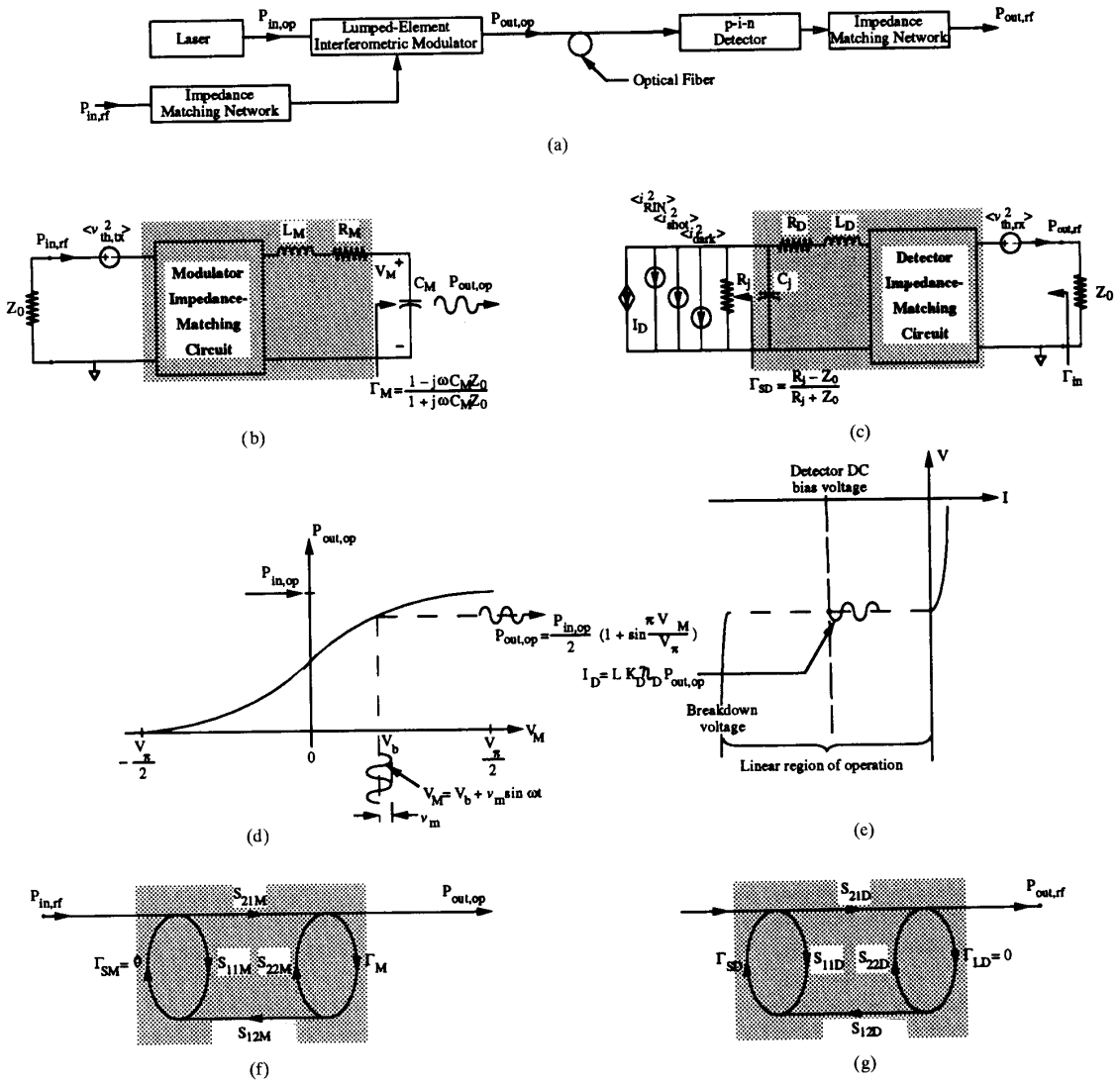

Fig. 1. Analytical model of external modulation fiber-optic link (after [4]): (a) schematic diagram; (b) equivalent circuit model of impedance-matched modulator in the optical transmitter; (c) equivalent circuit model of impedance-matched detector in the optical receiver; (d) relationship between optical output power and applied voltage for a Mach–Zehnder interferometric modulator; (e) relationship between optical input power and photocurrent for a reverse-biased p-i-n detector; (f) signal flow diagram for optical transmitter; (g) signal flow diagram for optical receiver.

II. Analysis

In [4], we derived a model for the microwave performance of the external modulation link shown in Fig. 1(a). We present the model here briefly, referring the reader to the earlier paper for more details.

In the external modulation link discussed in this paper, microwave modulation of a laser's optical output is accomplished using an impedance-matched $LiNbO_3$ Mach–Zehnder interferometric modulator. The model we describe is applicable only for frequencies at which the electrodes of the modulator can be considered lumped elements; that is, the electrodes must be short compared to the electrical wavelength of the modulating signal. For instance, this model applies to the modulator described in [4] because its electrodes are 0.050 in long—less than one-twentieth of a wavelength at the L-band frequency for which the modulator performance was optimized.

Device Characterization and Modeling

The generalized equivalent circuit diagrams for the modulator and detector are given in Fig. 1(b) and (c), respectively. The circuit elements for both the modulator (L_M, R_M, C_M) and the detector (R_j, C_j, R_D, L_D) are selected based on realistic physical models of the devices. In the case of the modulator, the electrodes across which we impose the microwave signal voltage V_M have capacitance C_M and resistive loss R_M, and are connected to the input circuit with a bondwire having inductance L_M. The detector is a reverse-biased p-i-n junction

with resistance R_j and capacitance C_j. Its electrodes, which have resistive loss R_D, are connected to the receiver circuit with bondwires of inductance L_D.

Using the Thru-Reflect-Line (TRL) de-embedding technique, we extract the intrinsic scattering parameters of the devices alone from the measured microwave impedances of the devices in their test fixtures [8]. Any of a number of available microwave CAD programs can then be used to select values for the equivalent circuit elements to fit the de-embedded microwave impedances. Once the devices have been modeled, the design of the circuits to match the modulator and detector impedances to the system impedance Z_0 (usually 50 Ω) can commence, and the gain, noise figure, and dynamic range of the link can be predicted.

Modulator Power versus Voltage (P–V) Relationship

For the lumped-element interferometric modulator, the relationship between the optical output power $P_{\text{out,op}}$, and the applied voltage V_M is shown in Fig. 1(d), where $P_{\text{in,op}}$ is the unmodulated optical power available at the electrodes of the modulator and V_π is the voltage required for full on-to-off switching. We generalize V_M as an RF modulation voltage $v_m \cdot \sin \omega t$ applied to a dc bias voltage V_b, where we have defined $V_b = 0$ as the quarterwave bias point in order to simplify our evaluation of the effects of nonquarterwave biasing.

Detector Power versus Current (P–I) Relationship

The ratio of detector photocurrent I_D to $P_{\text{out,op}}$ (the optical power at the output of the modulator) is $L\ K_D\ \eta_D$, where L is the total optical power loss due to attenuation in the fiber, K_D is the fiber-to-detector coupling efficiency, and η_D is the photodetector responsivity. This relationship is illustrated in Fig. 1(e). In the model which we describe in this paper, the detector is assumed to operate at a dc bias voltage which is large enough to ensure that it does not impose an upper limit on the RF power handling capability of the link. That is, even at 100% modulation depth in the modulator ($v_m = V_\pi/2$), the detector remains within its linear region of operation [as defined in Fig. 1(e)]. Additionally, we assume the detector operates at a frequency well below its 3-dB modulation bandwidth.

Gain Analysis

We calculate the gain of the external modulation fiber-optic link in terms of microwave scattering parameters using a signal flow diagram (SFD) technique. The SFD for the optical transmitter containing the lumped-element Mach–Zehnder interferometric modulator is obtained by considering the capacitance C_M across the modulator terminals to be the termination load Γ_M of a two-port network consisting of the microwave impedance-matching circuit and the other device parameters in the equivalent circuit of the modulator. This two-port network is denoted by the shaded region of the optical transmitter's equivalent circuit in Fig. 1(b). The SFD for the optical transmitter [Fig. 1(f)] replaces the circuit in the shaded region by its two-port microwave scattering parameters ($S_{11M}, S_{12M}, S_{21M}, S_{22M}$).

TABLE I
EQUATIONS FOR MODELING OF THE ANALOG SMALL-SIGNAL GAIN AND NOISE FIGURE OF AN EXTERNAL MODULATION FIBER-OPTIC LINK

Small-Signal Gain
$$G = \left(\frac{\pi P_{\text{in,op}} L K_D \eta_D Z_0}{2V_\pi}\right)^2 \cdot \frac{|S_{21M}|^2 |S_{21D}|^2 |1+\Gamma_M|^2}{|1-S_{22M}\Gamma_M|^2 |1-S_{11D}\Gamma_{SD}|^2} \cos^2 \frac{\pi V_b}{V_\pi} \cdot \quad (1)$$

Noise Figure
$$NF = \frac{(S/N)_{\text{input}}}{(S/N)_{\text{output}}} = \frac{P_{N,\text{out}}}{kT_a BG} \quad (2)$$

$$\text{where } P_{n,\text{out}} = N_{th,tx} + N_{th,rx} + N_{op} \quad (3)$$

$$\text{where } N_{th,tx} = \frac{\left\langle v_{th,tx}^2 \right\rangle B}{Z_0} G = 2kT_a BG \quad (4)$$

$$N_{th,rx} = \frac{\left\langle v_{th,rx}^2 \right\rangle B}{Z_0} = kT_a B\left(1 - |\Gamma_{\text{in}}|^2\right) \quad (5)$$

$$\text{and } N_{op} = \left[\langle i_{\text{RIN}}^2 \rangle + \langle i_{\text{shot}}^2 \rangle + \langle i_{\text{dark}}^2 \rangle\right] \frac{|S_{21D}|^2}{|1-S_{11D}\Gamma_{SD}|^2} BZ_0 \quad (6)$$

$$\text{where } \langle i_{\text{RIN}}^2 \rangle = \frac{1}{4}\left[P_{\text{in,op}} L K_D \eta_D \left(1 + \sin \frac{\pi V_b}{V_\pi}\right)\right]^2 \text{RIN}_{\text{laser}} \quad (7)$$

$$\langle i_{\text{shot}}^2 \rangle = e P_{\text{in,op}} L K_D \eta_D \left(1 + \sin \frac{\pi V_b}{V_\pi}\right) \quad (8)$$

$$\text{and } \left\langle i_{\text{dark}}^2 \right\rangle = 2eI_{\text{dark}} . \quad (9)$$

When a reverse-biases p-i-n photodiode is employed in the optical receiver, the SFD is obtained by considering the junction resistance of the diode to be the source termination Γ_{SD} of a two-port network consisting of the other device parameters of the photodetector and the microwave impedance-matching circuit. This two-port network is denoted by the shaded region of the optical receiver's equivalent circuit in Fig. 1(c). The SFD for the optical receiver [Fig. 1(g)] replaces the circuit in the shaded region by its two-port microwave scattering parameters ($S_{11D}, S_{12D}, S_{21D}, S_{22D}$).

Using the modulator P–V relationship, the detector P–I relationship, and the SFD's for the optical transmitter and receiver, we derived in [4] the expression for the small-signal gain G of the optical link. This is equation (1) of Table I. The $\cos^2(\pi V_b/V_\pi)$ term indicates how the gain of the external modulation link varies as a function of the modulator dc bias voltage.

Noise Analysis

The noise figure of any system is the extent to which the signal-to-noise ratio S/N deteriorates between input and output. At the input to the fiber-optic link, the noise power may be as low as the thermal noise limit, kT_aB, where k is Boltzmann's constant, T_a is the absolute ambient temperature, and B is the resolution bandwidth of the receiver. We define $P_{N,\text{out}}$ as the noise power at the output of the link. The noise figure NF is thus given by (2) in Table I.

As expressed in (3) of Table I, we consider the link output noise power $P_{N,\text{out}}$ to be the sum of the noise contributed by sources falling into three categories: $N_{th,tx}$, the thermal noise in the optical transmitter; $N_{th,rx}$, the thermal noise in

the optical receiver; and N_{op}, noise which occurs because we are communicating via an optical carrier.

The spectral densities of the thermal noise voltages at the input to the optical transmitter and the output of the optical receiver ($\langle \nu_{th,tx}^2 \rangle$ and $\langle \nu_{th,rx}^2 \rangle$, respectively) are shown in the equivalent circuit models of Fig. 1(b) and (c). Noise power from these sources is calculated by multiplying the noise voltage spectral densities by the receiver bandwidth B and dividing by the impedance Z_0 according to the Nyquist theorem [9]. We use the small signal gain equation (1) and Γ_{in}, the reflection coefficient looking into the receiver circuit from the link output, to calculate the contribution of these noise sources to the total link output noise [(4) and (5) of Table I].

The Nyquist theorem also allows us to represent the individual sources of optical noise contributing to N_{op} as equivalent noise current spectral densities in the optical receiver; these noise sources are shown in Fig. 1(c). By multiplying the total of these noise current spectral densities by the bandwidth, the impedance, and the transfer function of the receiver, we obtain the output noise power due to these sources [(6) of Table I]. As expressed in (6), the optical noise arises from these sources: $\langle i_{\text{RIN}}^2 \rangle$ is the noise current spectral density at the receiver due to the laser's relative intensity noise ($\text{RIN}_{\text{laser}}$); $\langle i_{\text{shot}}^2 \rangle$ reflects the shot noise of the photodiode; and $\langle i_{\text{dark}}^2 \rangle$ is the contribution from the photodiode's dark current, I_{dark}.

We derive the optical noise current spectral density expressions [(7), (8), and (9) of Table I] as follows. The dc component of modulator's optical output power $P_{\text{out,op}}$ is derived from the modulator P–V relationship when $\nu_m = 0$; that is [see Fig. 1(d)],

$$P_{\text{out},op}(\text{dc}) = \frac{P_{\text{in},op}}{2}\left(1 + \sin\frac{\pi V_b}{V_\pi}\right). \tag{10}$$

Therefore, from the detector's P–I relationship [Fig. 1(e)], we can also derive the dc photocurrent

$$I_D(\text{dc}) = \frac{LK_D\eta_D P_{\text{in},op}}{2}\left(1 + \sin\frac{\pi V_b}{V_\pi}\right). \tag{11}$$

The relative intensity noise of the laser is defined as the ratio of its optical noise power spectral density to its dc optical output power; the noise at the receiver due to $\text{RIN}_{\text{laser}}$ is, therefore,

$$\langle i_{\text{RIN}}^2 \rangle = [I_D(\text{dc})]^2 \text{RIN}_{\text{laser}} \tag{12}$$

and (7) in Table I is derived by substituting (11) into (12). Unlike the laser relative intensity noise, the shot noise and dark current noise arise due to the statistical nature of the production and collection of photoelectrons when an optical signal is incident on a photodetector, and are known to be Poisson processes [10] for which the noise spectral density is twice the product of the dc current and the electronic charge e. The noise current spectral densities due to shot noise and dark current in the receiver can therefore be calculated using, respectively, (8) and (9) of Table I, where the shot noise spectral density has been derived by substituting (11) into the following expression:

$$\langle i_{\text{shot}}^2 \rangle = 2eI_D(\text{dc}). \tag{13}$$

TABLE II
EQUATIONS FOR MODELING OF THE ANALOG SPURIOUS-FREE DYNAMIC RANGE AND COMPRESSION DYNAMIC RANGE OF AN EXTERNAL MODULATION FIBER-OPTIC LINK

Spurious-Free Dynamic Range

$$\text{SFDR} = \left(\frac{P_{\text{out},int}}{P_{N,\text{out}}}\right)^{\frac{2}{3}} = \left(\frac{P_{\text{in},int} \times G}{P_{N,\text{out}}}\right)^{\frac{2}{3}} = \left(\frac{P_{\text{in},int}}{kT_aBNF}\right)^{\frac{2}{3}} \tag{14}$$

$$\text{where } P_{\text{in},int} = \frac{8V_\pi^2|1 - S_{22M}\Gamma_M|^2}{\pi^2 Z_0|S_{21M}|^2|1 + \Gamma_M|^2}. \tag{15}$$

Compression Dynamic Range

$$\text{CDR} = \frac{1.259 \times P_{\text{out,1 dB CP}}}{P_{N,\text{out}}} = \frac{P_{\text{in,1 dB CP}} \times G}{P_{N,\text{out}}} = \frac{P_{\text{in,1 dB CP}}}{kT_aBNF} \tag{16}$$

$$\text{where } P_{\text{in,1 dB CP}} = \frac{(0.5500)^2 V_\pi^2|1 - S_{22M}\Gamma_M|^2}{\pi^2 Z_0|S_{21M}|^2|1 + \Gamma_M|^2}. \tag{17}$$

Distortion Analysis

In our derivation of the external modulation link gain, we assumed a small signal, i.e., $\nu_m << V_\pi/2$. As the input RF power is increased (and with it ν_m), the sinusoidal character of the modulator's P–V relationship eventually fails to approximate a linear response, resulting in AM compression and the generation of harmonics and intermodulation products.

We define the spurious-free dynamic range (SFDR) of an optical link as the range of input RF powers for which the fundamental signal power at the output is above the noise floor, but the third-order intermodulation product power is below the noise floor. This definition is expressed mathematically by (14) in Table II, in which $P_{\text{in,int}}$ and $P_{\text{out,int}}$ are the link input and output powers at the third-order intercept (where fundamental signal and third-order intermodulation product powers are equal).

We generalize the modulator voltage V_M as a two-tone modulating RF voltage $\nu_m(\sin\omega_1 t + \sin\omega_2 t)$ applied to a dc bias voltage V_b in order to determine $P_{\text{in,int}}$, the input power at which $P_{\text{out,op}}$ at third-order intermodulation frequency $2\omega_1 - \omega_2$ equals $P_{\text{out,op}}$ at fundamental frequency ω_1. This intercept point was derived in [4] and was found to be independent of the modulator dc bias voltage V_b, as shown by (15) in Table II.

The effect of AM compression is predicted in a similar fashion. We define the compression dynamic range (CDR) as the range of input RF powers for which the output signal power at the fundamental frequency is above the noise floor and is compressed by less than 1 dB relative to the small-signal response. This definition is expressed by (16) in Table II, in which $P_{\text{in,1 dB CP}}$ and $P_{\text{out,1 dB CP}}$ are the link input and output powers at the point where 1 dB of AM compression occurs. We derived $P_{in,1\text{ dB CP}}$ in [4] and found it to be independent of the modulator dc bias voltage V_b, as shown by (17) in Table II.

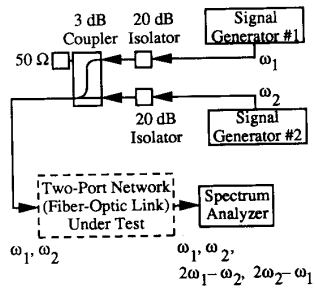

Fig. 2. Experimental setup for measuring the two-tone intermodulation distortion and output noise floor of the external modulation fiber-optic link.

III. Experimental Results

For the experimental external modulation link, we selected a 1.3 μm $LiNbO_3$ Mach–Zehnder interferometric modulator. The device exhibited a 23 dB extinction ratio when TE-polarized light was launched into its polarization-preserving input single-mode fiber pigtail, and had a switching voltage $V_\pi = 8.3$ V, a modulation bandwidth of 3 GHz, and 4.2 dB fiber-to-fiber optical insertion loss. An InGaAs p-i-n photodiode with a responsivity $\eta_D = 1.0$ A/W below a response bandwidth of 10 GHz was employed in the optical receiver. We developed equivalent circuit models using the de-embedded scattering parameters of the modulator and detector, and designed reactive circuits to impedance match the electro-optic devices to 50 Ω at the link's center design frequency of 900 MHz. In order to maximize the gain and dynamic range of the external modulation link, large optical pump power (30 mW at $\lambda = 1.3$ μm) was obtained from a single-mode fiber-pigtailed Nd:YAG laser with low RIN (-160 dB/Hz at 900 MHz). We optically coupled the solid-state laser and the optical receiver to the modulator's input and output fibers, respectively. The input polarization was adjusted to maximize the ratio of optical power measured at the on and off switch voltages.

We used an HP8510A automatic network analyzer and an HP8970B noise figure meter with an HP346C noise source to measure the link's small-signal gain and noise figure, respectively, at a variety of modulator bias voltages. Using the experimental set up shown in Fig. 2, we also measured the two-tone intermodulation distortion and the output noise floor of the fiber-optic link at its center frequency of 900 MHz for each of the modulator bias voltage levels at which we had measured gain and noise figure. The results of these measurements made it possible to determine, at each bias level, the measured spurious-free and compression dynamic ranges of the link (using (14) and (16) of Table II).

As we reproted in [4], the results at the modulator's quarterwave bias ($V_b = 0$) were as follows: $G = 0$ dB; $NF = 24.3$ dB; SFDR = 73.8 dB · $MHz^{2/3}$ (113.8 dB · $Hz^{2/3}$); CDR = 95.9 dB · MHz (155.9 dB · Hz). We found, however, that at $V_b = -2.3\ V \approx -0.3V_\pi$, even though gain degraded to -3.6 dB, noise figure improved to 21.2 dB. In Fig. 3, we have plotted the output powers of the fundamental signal, third-order intermodulation product, and noise as a function of the input fundamental signal power (as measured using the setup

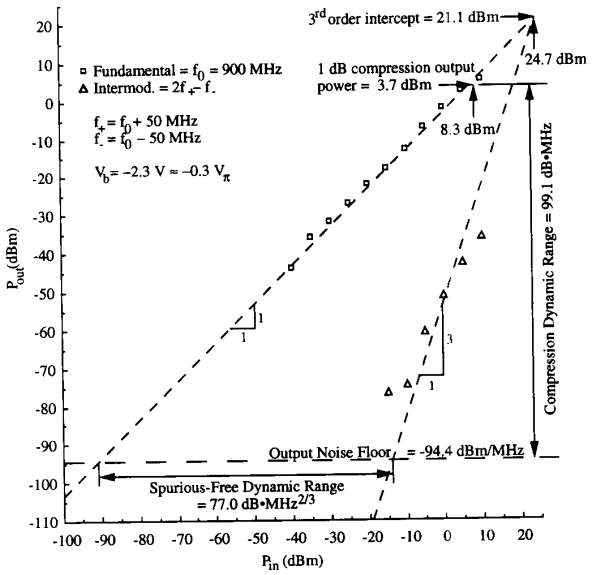

Fig. 3. Result of a two-tone intermodulation distortion measurement, showing the 1 dB compression and third-order intercept points of the external modulation link at a modulator bias voltage of $V_b = -2.3$ V. The link's 99.1 dB · MHz compression dynamic range and spurious-free dynamic range of 77.0 dB · $MHz^{2/3}$ are rendered as well.

in Fig. 2 with a fundamental tone separation of 100 MHz) for the $V_b = -2.3$ V case. The measured 1 dB compression and third-order intercept output powers are 3.7 and 21.1 dBm, respectively. Thus, the compression dynamic range at this bias point is 99.1 dB · MHz (159.1 dB · Hz) and the spurious-free dynamic range is 77.0 dB · $MHz^{2/3}$ (117.0 dB · $Hz^{2/3}$), which is, to our knowledge, the largest dynamic range reported to date for any microwave fiber-optic link.

IV. Verification of the Analytical Bias-Dependent Model

The measured 900 MHz gain and noise figure of the fiber-optic link are plotted as a function of V_b in Fig. 4. This graph also shows the gain and noise figure we predict by substituting the model's 900 MHz S-parameters and measured values of $P_{in,op}$, L, K_D, η_D, V_π, V_b, Γ_{in}, RIN_{laser} and I_{dark} into (1)–(9) of Table I. Knowing these parameters also allows us to predict values for the 1 dB compression, third-order intercept, and noise output powers, from which we calculate the expected compression and spurious-free dynamic ranges. In Fig. 5, we plot these predictions as a function of the modulator bias V_b, and compare them to the dynamic ranges that we calculate from the results of our intermodulation distortion and noise floor measurements.

We notice in Fig. 5 that the spurious-free dynamic range calculated from predicted intercept and noise powers consistently falls 1–3 dB short of the SFDR calculated from the intermodulation distortion and noise floor measurements. This discrepancy may be due to the link's very narrow (50 MHz) 3-dB bandwidth. That is, the measured intermodulation distortion products are suppressed somewhat by the very narrow

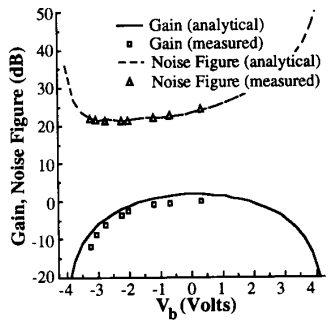

Fig. 4. Gain and noise figure of the experimental external modulation link at $f = 900$ MHz as a function of the modulator bias voltage. Measured and analytically determined values are shown.

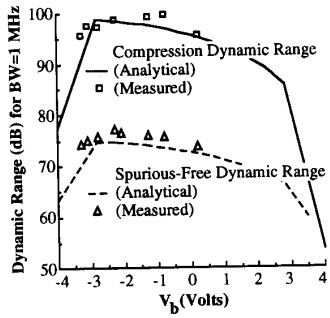

Fig. 5. Compression and spurious-free dynamic range of the experimental external modulation link at $f = 900$ MHz as a function of the modulator bias voltage. Measured and analytically determined values are shown.

bandpass filters in both the modulator and detector matching circuits, resulting in an artificially high interpretation of the third-order intercept output power. The minor inaccuracy may also result from the fact that our intermodulation distortion and AM compression predictions were based on a modulator with an optical output power $P_{\text{out,op}}$ that varies sinusoidally with bias voltage V_b as shown in Fig. 1(d). We observed in our measurements that the $P-V$ characteristic of our modulator deviated 5–10% from perfectly sinusoidal behavior.

Even though it fails to match the measured results exactly, our analytical model does allow us to predict correctly that the lowest noise figure and highest dynamic range is measured when the modulator bias voltage is −2.3 V, or approximately $-0.3\ V_\pi$ (see Fig. 4 and 5). In the discussion which follows, we exploit the model to investigate why our experimental link performs optimally at this bias level, and to what extent the performance can be improved.

V. Discussion of the Bias Dependent Performance

The external modulation link's small signal gain is optimum at the modulator's quarterwave bias point ($V_b = 0$) because the slope of the modulator's output versus input characteristic is maximum at this point [see Fig. 1(d)]. This gain maximum at $V_b = 0$ is reflected in the model by the bias-dependent coefficient $\cos^2(\pi V_b/V_\pi)$ in (1) of Table I, and is reflected in our link's measured performance as well (see Fig. 4).

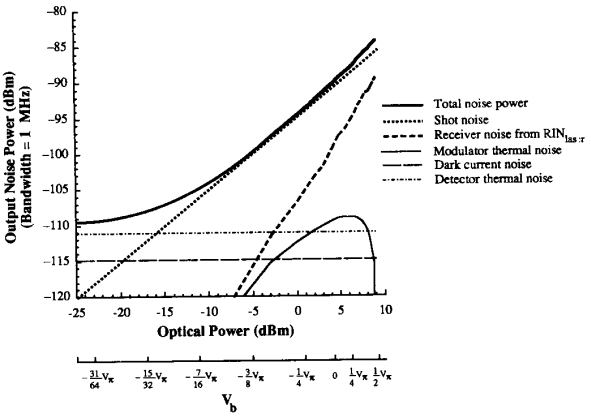

Fig. 6. Sources of noise contributing to the measured output noise floor (at $f = 900$ MHz) of the experimental external modulation link, plotted as a function of both the modulator bias voltage and the optical power detected in the optical receiver.

According to (15) and (17) of Table II, the input power at which the link's third-order intercept and 1 dB compression points occur is invariant with the modulator bias V_b. When we derived these equations in [4], we found that the AM compression and third-order intermodulation distortion effects increase as $\cos^2(\pi V_b/V_\pi)$—the same rate at which the fundamental signal gain decreases—resulting in no net change in $P_{\text{in,int}}$ and $P_{\text{in,1 dB CP}}$. Thus, the final expressions in (14) and (15) dictate that the spurious-free and compression dynamic ranges are maximum at the modulator bias where the noise figure is minimum, as we have verified experimentally (see Figs. 4 and 5).

Equation (2) indicates that this optimum bias point must lie somewhere between $V_b = 0$, where gain is maximum, and a point near the halfwave voltage $V_b = -V_\pi/2$, where $P_{N,\text{out}}$ is its minimum value. The exact value of this optimum modulator bias voltage depends upon all the variables in (1)–(9). The model allows us to use these equations to determine how the optimum V_b changes with any of these variables. As an example, we have investigated the effect of the available laser power $P_{\text{in,op}}$.

The relative contributions of the different sources of noise in the external modulation link vary with the optical power detected in the receiver, which is a sinusoidal function of the modular dc bias voltage. In Fig. 6, we show the calculated contributions to the output noise floor of the link model at $f = 900$ MHz, plotted as a function of both the detected optical power and the V_b setting. Shot noise increases linearly with the dc optical power impinging on the photodetector, whereas noise in the receiver due to $\text{RIN}_{\text{laser}}$ increases as the square of optical power. Modulator thermal noise is proportional to the microwave-modulated optical power, and the remaining noise contributions (detector dark current and thermal noise) are independent of the optical power.

Provided that the optical source is a solid-state laser with low RIN, the shot noise in the external modulation link is always more significant than the noise due to $\text{RIN}_{\text{laser}}$. As $P_{\text{in,op}}$ is increased by using higher-power optical sources,

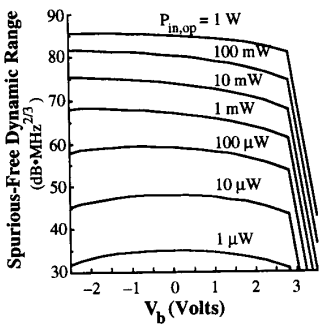

Fig. 7. Calculated spurious-free dynamic range of the 900 MHz external modulation link as a function of the modulator bias voltage, plotted for several assumed levels of available optical power.

modulator thermal noise eventually overtakes the shot noise due to the increased link gain, and biasing the modulator even closer to the halfwave voltage is necessary to reduce the output noise floor to its minimum value. Thus, the bias point at which maximum dynamic range is achieved approaches $-V_\pi/2$ asymptotically as larger optical source power is made available. An important tradeoff exists, since gain is always greatest at the linear bias point $V_b = 0$.

We have used our model to calculate the experimental link's spurious-free dynamic range for several assumed levels of available optical power $P_{\text{in,op}}$. In Fig. 7, we plot these predictions as a function of the modulator bias V_b. As the plot shows, between the halfwave and quarterwave modulator bias points, the dynamic range varies less with larger optical source powers. For larger optical source powers, there is thus a less severe tradeoff between gain and noise figure, i.e., at the quarterwave bias point both are excellent.

If a high-power low-RIN solid-state laser can be used without damaging the modulator or detector, and if the detector has very low dark current, then near the modulator's halfwave voltage $(-V_\pi/2)$

$$P_{N,\text{out}} \rightarrow 2kT_aBG\,, \tag{18}$$

and

$$NF \rightarrow 2\,. \tag{19}$$

The lowest possible external modulation link noise figure is therefore 3 dB, as has already been claimed [2]. Since at high optical source powers the external modulation link noise figure varies only slightly with V_b between 0 and $-V_\pi/2$, even at the quarterwave bias voltage the noise figure approaches 3 dB, and the dynamic ranges approach their theoretical limits, i.e.,

$$\text{SFDR} \rightarrow \left(\frac{4V_\pi^2|1 - S_{22M}\Gamma_M|^2}{\pi^2 kT_aBZ_0|S_{21M}|^2|1+\Gamma_M|^2}\right)^{\frac{2}{3}} \tag{20}$$

and

$$\text{CDR} \rightarrow \frac{0.1513V_\pi^2|1 - S_{22M}\Gamma_M|^2}{\pi^2 kT_aBZ_0|S_{21M}|^2|1+\Gamma_M|^2}\,. \tag{21}$$

The absolute upper limit to the spurious-free and compression dynamic ranges of our 900 MHz experimental external modulation link are, therefore, 86.8 dB · $MHz^{2/3}$ (126.8 dB · $Hz^{2/3}$) and 176.0 dB· MHz (106.0 dB · Hz), respectively.

Equations (20) and (21) illustrate that, conversely to the link gain—which is optimum when the modulator capacitance, resistance, and switching voltage are minimized—the dynamic range upper limit can only be increased by increasing these same parameters. The optimum dynamic range is approached, however, only when gain is maximized. Therefore, the gain/dynamic range tradeoff and how it may be controlled by varying the modulator bias voltage must be understood when attempting to design an external modulation fiber-optic link to meet stringent performance specifications.

VI. Conclusions

We have presented and experimentally verified a complete model of external modulation fiber-optic link performance. The potential for very high gain and wide dynamic range has been demonstrated by the experimental external modulation link, which features a peak gain of 0 dB and compression and spurious-free dynamic ranges of 99.1 dB · MHz and 77.0 dB · $MHz^{2/3}$, respectively. The model has anticipated the fact that the measured dynamic ranges are 2–3 dB larger when our modulator is biased near the halfwave voltage $(V_b = -V_\pi/2)$ than at the quarterwave bias $(V_b = 0)$ where gain is maximum. Operation of the modulator near the halfwave bias voltage offers the additional advantages of minimizing the link noise figure and shielding the detector from large incident optical intensity, with the drawback being reduced link gain. The model proves that this tradeoff is least severe when the available optical source power is maximized; however, the optical power may be limited by the devices or by the desire to distribute the output of one solid-state laser source to many coherent fiber-optic links. Thus, it is important for the system designer to be cognizant of the dependence of all these performance parameters upon the modulator bias voltage.

References

[1] E. Ackerman, S. Wanuga, K. Candela, R. Scotti, W. MacDonald, and J. Gates, "A 3 to 6 GHz microwave/photonic transceiver for phased-array interconnects," *Microwave J.*, vol. 35, no. 3, pp. 60–71, Apr. 1992.

[2] G. E. Betts, L. M. Johnson, C. H. Cox, III, and S. D. Lowney, "High-performance optical analog link using external modulator," *IEEE Photon. Technol. Lett.*, vol. 1, pp. 404–406, Nov. 1989.

[3] G. E. Betts, C. H. Cox, III, and K. G. Ray, "20-GHz optical link using an external modulator," *IEEE Photon. Technol. Lett.*, vol. 2, pp. 923–925, Dec. 1990.

[4] A. S. Daryoush, E. Ackerman, N. R. Samant, S. Wanuga, and D. Kasemset, "Interfaces for high-speed fiberoptic links," *IEEE Trans. Microwave Theory Tech.*, vol. 39, pp. 2031–2044, Dec. 1991.

[5] B. H. Kolner and D. M. Bloom, "Electrooptic sampling in GaAs integrated circuits," *IEEE J. Quantum Electron.*, vol. QE-22, pp. 79–93, Jan. 1986.

[6] C. H. Bulmer and W. K. Burns, "Linear interferometric modulators in Ti:$LiNbO_3$," *IEEE J. Lightwave Technol.*, vol. LT-2, pp. 512–521, Aug. 1984.

[7] B. H. Kolner and D. W. Dolfi, "Intermodulation distortion and compression in an integrated electrooptic modulator," *Appl. Opt.*, vol. 26, no. 17, pp. 3676–3680, Sept. 1987.

[8] G. F. Engen and C. A. Hoer, "Thru-reflect-line: An improved technique for calibrating the dual 6-port automatic network analyzer," *IEEE Trans. Microwave Theory Tech.*, vol. MTT-27, pp. 983–987, Dec. 1979.

[9] A. Papoulis, *Probability, Random Variables, and Stochastic Processes*. New York: McGraw-Hill, 1965, pp. 138–141.

[10] B.M. Oliver, "Thermal and quantum noise," *Proc. IEEE,* vol. 53, pp. 436–454, May 1965.

Edward Ackerman (S'86–S'87–M'87–M'89) received the B.S. degree in electrical engineering from Lafayette College, Easton, PA, and the M.S. degree in electrical engineering from Drexel University, Philadelphia, PA. He is currently pursuing the Ph.D. degree at Drexel University.

He is employed as a Microwave Engineer at GE Electronics Laboratory, Syracuse, NY, where he is developing high-fidelity photonic systems for microwave and millimeter-wave communication applications.

Stephen Wanuga (S'58–M'60–SM'85–F'92) received the B.S.E.E. degree from Pennsylvania State University in 1959 and the M.S.E.E. degree from Syracuse University in 1967.

He is with the General Electric electronics Laboratory, Syracuse, NY, where he has been responsible for development of various solid-state acoustic, microwave and optoelectronic devices and components. Currently he is Project Leader on research and development of broad-band low-loss microwave photonic links and components for phased array radar and communication systems.

Dumrong Kasemset (M'82) received the S.B., S.M., and Ph.D. degrees from the Massachusetts Institute of Technology, Cambridge, all in electrical engineering, in 1977, 1979, and 1981, respectively.

In 1989 he joined the staff of GE's Electronic Laboratory, Syracuse, NY, where he was Manager of Integrated Optoelectronics Programs for GE Aerospace. Currently he is living in Thailand.

Afshin S. Daryoush (S'84–M'86–SM'91) was born in Iran in 1957. He received the B.S. degree in electrical engineering in 1981 from Case Western Reserve University, Cleveland, OH, and the M.S. and Ph.D. degrees in 1984 and 1986, respectively, from Drexel University, Philadelphia, PA, also in electrical engineering.

After graduation he joined the staff of Drexel University, first as Research Assistant Professor and then, beginning in 1987, as DuPont Assistant Professor of Electrical and Computer Engineering. In 1989 he was promoted to Associate Professor. He has conducted research in the area of optically controlled microwave devices and subsystems, high-speed fiber-optic links, and system studies of large-aperture phased array antennas. During the summers of 1987 and 1988, he was a Summer Faculty Fellow at NASA, Lewis Research Center, Cleveland, OH, conducting research on high-speed LEDs for 1.25 Gb/s fiber-optic links for computer backplanes at the Naval Air Development Center, Warminster, PA. He has authored or coauthored over 90 technical publications in the areas of light interaction with passive and active microwave devices, circuits, and systems. He has lectured frequently at workshops and international symposia.

Dr. Daryoush is recipient of the Microwave Prize from the 16th European Microwave Conference, Dublin, Ireland; he also received the best paper award at the IMPATT Session of the 1986 International Microwave Symposium, Baltimore, MD. He has also been awarded a U.S. patent on the optically controlled patch antenna. He is a member of Sigma Xi.

Niranjan R. Samant (S'90) was born in Bombay, India, in 1968. He received the B.E. degree in electronics and communicaions engineering from the Mangalore University, India, and the M.S. degree in electrical engineering from Drexel University, Philadelphia, PA.

His research interests include design and analysis of fiber optic links. Currently he is employed as an Engineer at Jaret Communications, Philadelphia, PA.

Mr. Samant is a member of the IEEE Microwave Theory and Techniques Society.